



Phosphomolybdic acid embedded into biomass-derived biochar carbon electrode for supercapacitor applications



Madhusree J.E.^a, Pranay R. Chandewar^b, Debaprasad Shee^b, Sib Sankar Mal^{a,*}

^a Materials and Catalysis Laboratory, Department of Chemistry, National Institute of Technology Karnataka, Surathkal 575025, India

^b Department of Chemical Engineering, Indian Institute of Technology Hyderabad, Kandi, Sengareddy 502284, Telangana, India

ARTICLE INFO

Keywords:

Orange peels

Activated carbon

Phosphomolybdic acid

Electrochemical impedance spectroscopy

ABSTRACT

In high-performance, clean, safe, and cost-effective ways, supercapacitors are among the most promising ways to store and release nonfossil energy. In recent years, renewable biomass-derived activated carbon has been explored as a potential option for electrode material. It restricts their specific capacitance despite being environment-friendly and possessing intrinsic mechanical strength. In order to overcome this limitation and preserve all other properties, we are infusing polyoxometalate into the activated carbon; this increases specific capacitance with its fast reversible redox behaviour and preserves the carbon's characteristics. Beside suffusing phosphomolybdic acid (PMA) into biomass waste material, such as orange peel-derived activated carbon (OPAC), a new hybrid material (OPAC-PMA) was developed. The nanohybrid design was revealed by structural and morphological research, which showed high interfacial contact, allowing polyanions to redox rapidly. The novel hybrid electrode material (OPAC-PMA) has a capacitance value of 66% higher than the bare OPAC electrode. A further study showed that OPAC-PMA composite showed 88.23% cycle stability in 0.5 M H₂SO₄ electrolyte at 6 A g⁻¹ for 4000 cycles.

1. Introduction

In recent decades, energy storage has become one of the top precedents due to the unpredictability of renewable energy sources [1]. Although utilization of various renewable energy sources is gradually increasing despite some inherent limitations. Renewable energy causes such as solar and wind rely heavily on environmental conditions and inconsistent wind velocity and direction [2]. A high-performance energy storage device to store the energy generated is a prerequisite and should stabilize the associated power grid to overcome the present situation. Electrochemical energy storage devices have the potential to be useful as additional supplementary facilities. Researchers have been attempting to extract energy using electrochemical devices such as batteries [3], capacitors [4], fuel cells [5], and supercapacitors [6,7]. These supercapacitors have harvested substantial consideration in energy technology by achieving high power density with a satisfactory life cycle, fast charge, and discharge cycle compared to batteries. During the past few decades, scientists have worked hard to build SCs that are as reliable and powerful as batteries while maintaining high power output and cycle stability [8]. In computing, SCs can be categorized into pseudocapacitors and electric double-layer capacitors (EDLC).

In EDLC, carbonaceous nanostructures have found extensive use in electrodes due to several characteristics. These include a large surface area with adjustable porosity, high conductivity, high mechanical and electrochemical stability, ease of production, and inexpensive cost [9]. Through EDLC-based SC applications, graphene oxides (GO) [10], reduced graphene oxides (RGO) [11], activated carbons (AC) [12], and carbon nanotubes (CNTs) [13] have been extensively explored. Among all materials, it is commonly acknowledged that activated carbon obtained from biomass has enormous potential for extracting value from waste. Renewable source biomass and its derivatives have recently been explored as prospective options to replace existing non-sustainable electrode materials due to their inherent traits and benefits, including environment-friendly characteristics, various architectures, intrinsic mechanical strength and flexibility, and the capacity to accept additional functional materials efficiently [14]. In the recent period, substantial attempts have been made for the sustainable development of high-performance biomass-derived electrode materials [15]. All biomass materials are composed of hemicellulose, lignin, and cellulose, which can be used to manufacture porous carbon for supercapacitors, e.g., wood, fruit shells, plants, and animal tissues [16]. Several studies have described the synthesis of carbon from

* Corresponding author.

E-mail address: mals@nitk.edu.in (S. Sankar Mal).

organic waste materials such as groundnut peel [17–18], banana peel [19–20], pomegranate peel [21–22], and coconut shell [23–24], bamboo [25–26], wood [27–28], dead ginkgo leaves [29] and among others, where these items are utilized entirely to get carbon. Still, their specific capacitance value is relatively confined because of their charge storage system (EDLC) [30].

On the contrary, pseudocapacitors can generate high specific capacitance because of their unique electrochemical behaviour. The pseudo capacitor's performance is attributed to its electrode material, which experiences a rapid and reversible redox reaction with the generation of free ions [31–33]. Although these pseudocapacitive materials (conducting polymers, metal oxides, polyoxometalates, and sulphides) exhibit improved electrochemical performance, they experience material deterioration over lengthy cycle life, high cost, and mechanical stability [34]. A novel hybrid materials genre is needed to counterbalance the drawbacks of both categories of electrode materials. The combination of carbon and polyoxometalate appears to be solely compatible; it affords a good combination of both EDLC and faradic behaviour [35].

Polyoxometalate (POM), on the other hand, is an inorganic metal–oxygen cluster that has emerged as an intriguing choice for developing nanocomposite materials with specialized characteristics and increased functionality [36–38]. These are massive metal oxide clusters of early transition elements that vary in shape, size, and composition. Among the various forms of POM compounds, the Keggin cluster has received the most attention owing to its thermal stability and ease of synthesis $[MX_{12}O_{40}]$ [39]; M is a heteroatom, while X is an addenda atom. The addenda atom is an early transition metal such as Mo, W, or V. POMs can undergo reversible multi-electron transfer processes, making them excellent redox stability. The capacity of the electrode surface to absorb 24 electrons reversibly improves wettability with electrolytes [40–41].

Based on this concept, in 2017, Lian and co-workers first demonstrated the POM-mediated biomass-derived activated carbon for energy application using 3-electrodes systems. Activated carbon derived from pinecones was anchored with phosphomolybdic acid. The electrochemical performance of the composite materials was studied in 1 M H_2SO_4 and observed a specific capacitance of $361 F g^{-1}$ at $10 mV s^{-1}$ [42]. These results motivated us to examine further POM-modified biomass-derived activated carbon for supercapacitor applications in detail using a 2-electrode system.

A new report by the agricultural department reported an increase in orange production globally, resulting in a greater variety of orange peels. This is one of the cheapest materials discarded in the juice/fruit stands and can be used as a low-cost biomaterial compared to other materials such as bamboo and wood [43,44]. Here we report on the combination of orange peels derived activated carbon (OPAC) and $H_3[PMo_{12}O_{40}].12H_2O$, denoted as (PMA) for supercapacitors application in detail. In this paper, we have successfully synthesized the activated carbon from orange peel (OPAC) by a 1:3 KOH activating agent. Further, phosphomolybdic acid (PMA) was incorporated into the carbon surface and was confirmed by FESEM. The OPAC-PMA composite exhibits $126 F g^{-1}$ with specific energy and power density of $17.55 Wh kg^{-1}$ and $2000 W kg^{-1}$ compared to the bare OPAC, which gives $41.6 F g^{-1}$, an energy and power density of $5.77 Wh kg^{-1}$ and $1999 W kg^{-1}$ at $1 A g^{-1}$ in a symmetric cell.

2. Materials and methods

Orange peels were purchased from the local market in Mangalore, Karnataka, India. Phosphomolybdic acid, and N-1-Methyl-2-pyrrolidone (NMP), were purchased from Sigma Aldrich. Sulfuric acid (H_2SO_4), Distilled water, and HPLC-grade water were purchased from Loba Chemicals. Alfa Aesar provided polyvinylidene fluoride (PVDF). In this study, all analytical grade reagents were utilized without further purification.

2.1. Pyrolysis of orange peels produces activated carbon (OPAC)

The activated carbon from orange peels was prepared following the reported synthesis process described elsewhere [45]. The schematic representation of activated carbon synthesis from orange peels is shown in Fig. 1. After collecting orange peels, it was washed thoroughly with water to remove dirt, dried under sunlight, and ground into fine powder. The powdered orange peel was pre-carbonized for 4 h at $550 ^\circ C$ in a tubular furnace under a nitrogen atmosphere. The resultant carbon material was chemically activated using KOH. During the chemical activation process, a mixture of powdered carbon material (1 g) and pelleted KOH (3 g) taken in a ratio of 1:3 was heat treated at $800 ^\circ C$ for 1 h in a flowing of nitrogen in a tube furnace. The KOH-activated carbon material was ground into powder, treated with 1 M HCl, washed thoroughly with distilled water, and dried at $110 ^\circ C$ overnight in a hot air oven. The obtained activated carbon sample was named OPAC.

2.2. Preparation of molybdophosphoric acid–Orange peel-derived activated carbon nano hybrids

The phosphomolybdic acid (40 wt%) was dissolved in 2 ml of distilled water taken in a glass vial. The required amount of OPAC (60 wt %) was born in a round bottom flask. Then the prepared aqueous phosphomolybdic acid (PMA) solution was slowly added to it (Fig. 2). The resulting solution was continued stirring for 24 h at room temperature. The obtained black residue was filtered and washed thoroughly with HPLC-grade water until a clear filtrate was obtained. The black OPAC-PMA was collected and dried before use.

2.3. Preparation of electrode

First, 90% of fine powdered active materials (OPAC-PMA) were mixed with 10% PVDF and 2 ml of NMP (N-Methyl-2- Pyrrolidone) to make a slurry. Next, the slurry was kept for sonication for about $1\frac{1}{2}$ hr to disperse the electrode materials. A $1 cm \times 1 cm$ carbon cloth (mass of active material 0.9 mg) was gently and uniformly coated with the prepared slurry using a micropipette. The electrode material coated carbon cloth was dried at $65 ^\circ C$ for over 24 h and used as an electrode for the present study.

2.4. Device fabrication

The electrodes were fabricated into a symmetric 2-electrode setup utilizing a stainless-steel split cell. Both sides of the electrodes were attached to the current collector, with the coated side facing the separator (Whatman filter paper). An aqueous electrolyte was applied to the entire setup and tested for electrochemical performance.

3. Result and discussion

3.1. FTIR

Fourier transforms infrared (FTIR, a Bruker 4000 (USA) spectrometer) spectroscopy was used to investigate the successful deposition of PMA on activated carbon; Fig. 3 illustrates the FTIR spectra of bare orange peel-derived activated carbon (OPAC), pure PMA ($H_3[PMo_{12}O_{40}].12H_2O$), and composite materials such as OPAC-PMA. In both PMA and OPAC, the FTIR bands correlate well with the literature. The FTIR bands of the PMA compound that appeared at 1062, 966, 867, and $797 cm^{-1}$ originated because of the vibration of the P–O, terminal Mo–O, corner Mo–O, and edge Mo–O bonds [46]. Similarly, IR bands at $3400 cm^{-1}$, $1587 cm^{-1}$, and $1407 cm^{-1}$ denote the presence of the O–H group, C–O group, and C–C, respectively. The IR band at $1105 cm^{-1}$ indicates the presence of the carboxylic group

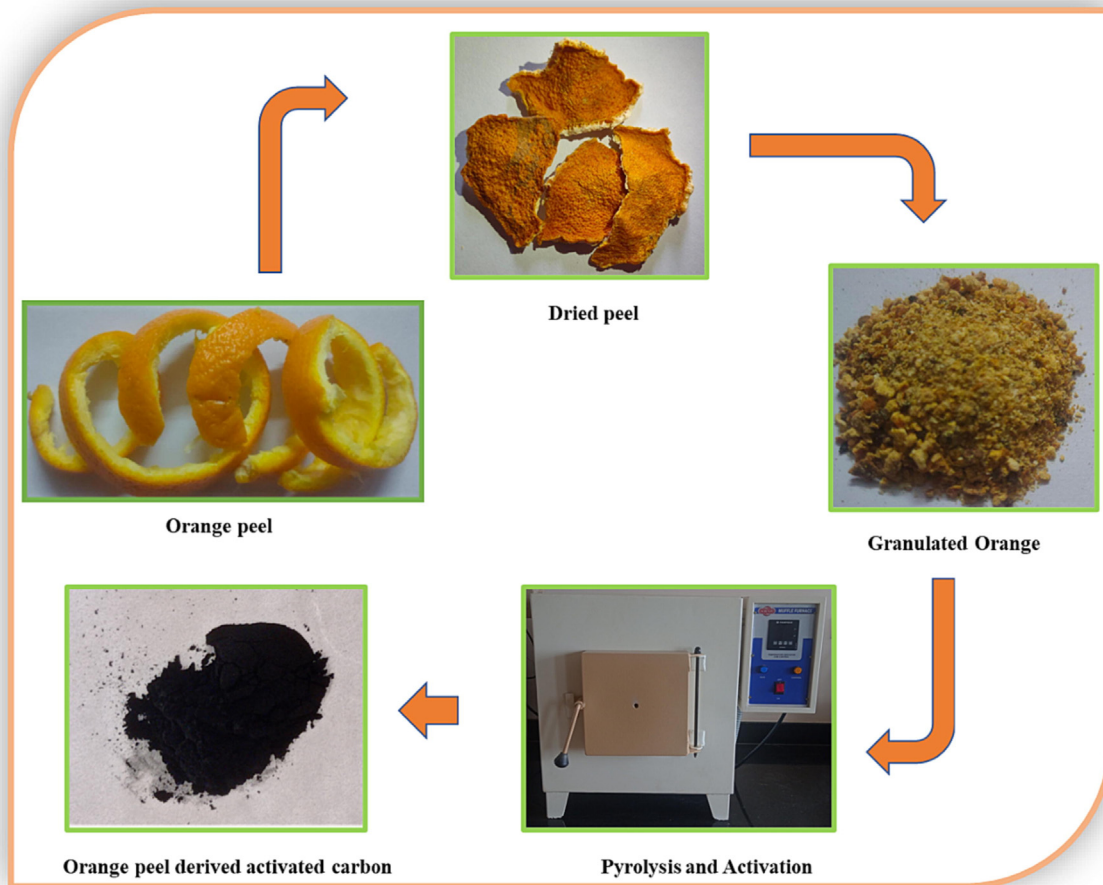


Fig. 1. Schematic representation of orange peel-derived activated preparation. (For interpretation of the references to colour in this figure legend, the reader is referred to the web version of this article.)

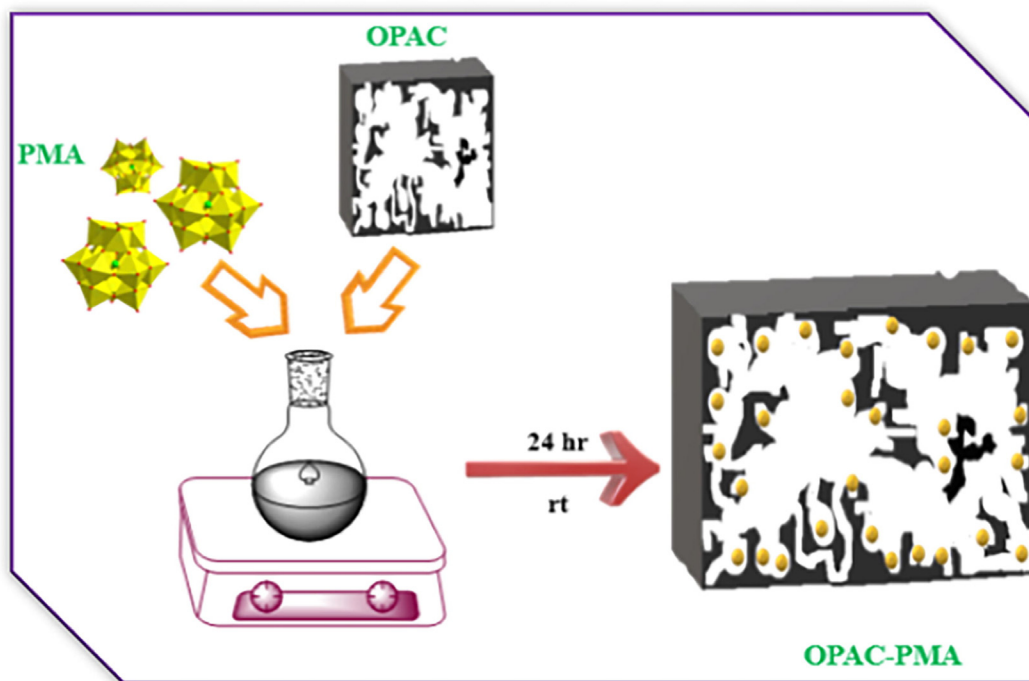


Fig. 2. Schematic representation of the synthesis of infusing Phosphomolybdic acid into orange peel-derived activated carbon. (For interpretation of the references to colour in this figure legend, the reader is referred to the web version of this article.)

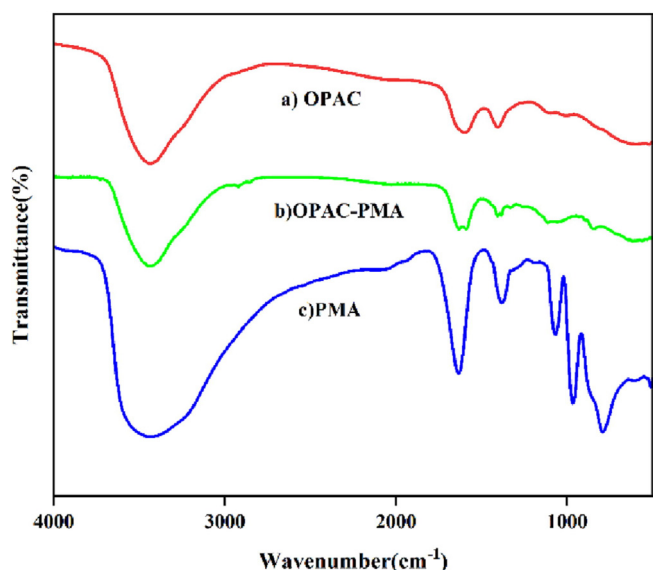


Fig. 3. FTIR Spectra of OPAC, OPAC-PMA, and PMA.

[47]. The various IR bands observed in OPAC, PMA, and OPAC-PMA are presented in Table S1.

3.2. Thermogravimetric analysis

The composite's thermogravimetric analysis (PerkinElmer TGA 4000) shows (Fig. 4) that doping redox-active PMA enhance the electrode's thermal stability. The thermal stability of the OPAC and OPAC-PMA was determined in the temperature ranging from room temperature to 900 °C at a scan rate of 10 °C (Fig. S1a). The DTG curve of OPAC-PMA depicts a water loss of 24% weight until 76.6 °C (Fig. S1b). The second stage weight loss of ~ 3% weight was observed at 551.5 °C, as shown in the DTG curve, which was attributed to the removal of structural water and the Keggin unit [48]. The OPAC released moisture at 71.36 °C resulting in a weight loss of 21.05%. Fig. S1(c&d) shows further weight losses of 3 % at 288.41 °C, which resembles the organic carbon structures, and a final loss of 2.6 % at 714.77 °C due to either oxides or inorganic impurities, which corroborating the reported study [49,50].

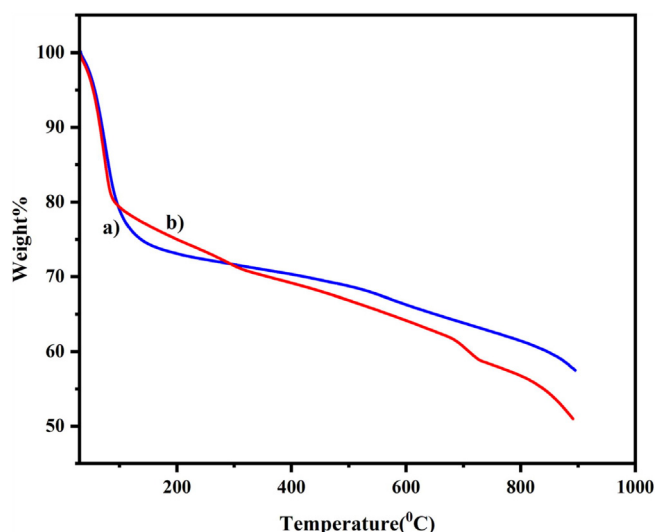


Fig. 4. The TGA graph of a) OPAC-PMA and b) OPAC.

3.3. XRD analysis

The XRD (Rigaku Smart lab (Japan)) patterns of OPAC and OPAC-PMA composite are presented in Fig. 5. The OPAC demonstrates a broad, amorphous nature peak, as shown in Fig. 5a. The broad peaks showed around 24.0° (002) and 43.8° (100) are attributed to the graphitic carbon [51]. Due to the incorporation of PMA into the OPAC, the OPAC-PMA composite exhibits both amorphous and crystalline properties. The PMA features were confirmed by the JCPDF (00-043-0316).

3.4. XPS analysis

The electronic state of constituent elements on the surface was determined using XPS (X-ray photoelectron spectroscopy, ThermoFisher scientific: Nexsa G2base). The individual XPS spectra of constituent elements of OPAC-PMA nanocomposites are presented in Fig. 6. However, the overall XPS survey scan for the OPAC-PMA composite is shown in Fig. S2. The C1s spectra of the OPAC-PMA nanocomposite revealed several peaks corresponding to element carbons of different characteristics, such as C=C at 284.5 eV, C—O—C at 285.4 eV, and C=O at 289.4 eV (Fig. 6b) [52]. The O1s spectra revealed peaks for O atoms of the different environments at 532.1 eV for C—O (O₁), 533.6 eV for C=O (O₂), and 536 eV for H—O (O₃), and 529–530 eV for metal oxide (O₄) as shown in Fig. 6b, [52]. Conversely, the OPAC-PMA nanocomposite exhibited two distinct peaks corresponding to 3d_{3/2} and 3d_{5/2} of Mo (+6) at 232.8 eV and 236.0 eV, respectively, as shown in Fig. 6c [53]. The deconvoluted P spectra showed (Fig. 6d) a 2p peak at 135.2 eV assigned to the P atom (+5) in the Keggin anion. [53].

3.5. Morphological studies

The FESEM (Carl Zeiss Sigma FESEM, Germany) images of OPAC and OPAC-PMA composite electrode materials are presented in Fig. 7. FESEM imaging enables us to contrast the surface morphology between the two electrode materials. Fig. 7(a) shows the porous nature of OPAC, which is reminiscent of a honeycomb structure with a 7.5 μm size. Similarly, Fig. 7(b) represents the surface morphology of the composite (OPAC-PMA), which shows the deposition of PMA with a size of approximately 2 nm and fits into the OPAC pores. FESEMs of OPAC

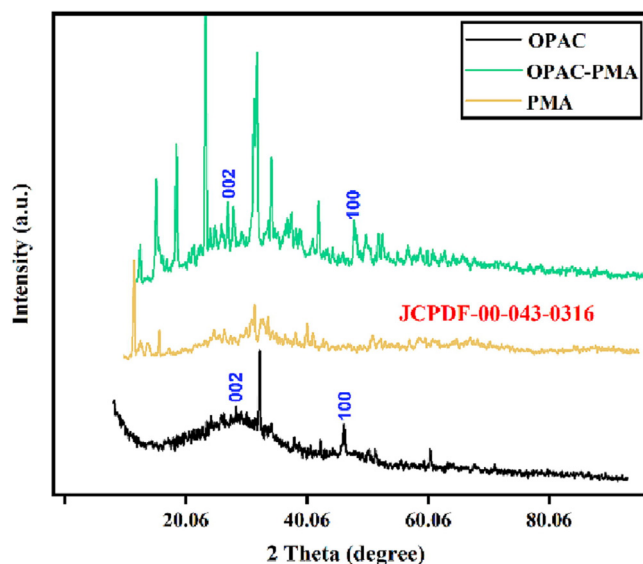


Fig. 5. a) Powder XRD spectrum of OPAC, PMA and OPAC-PMA.

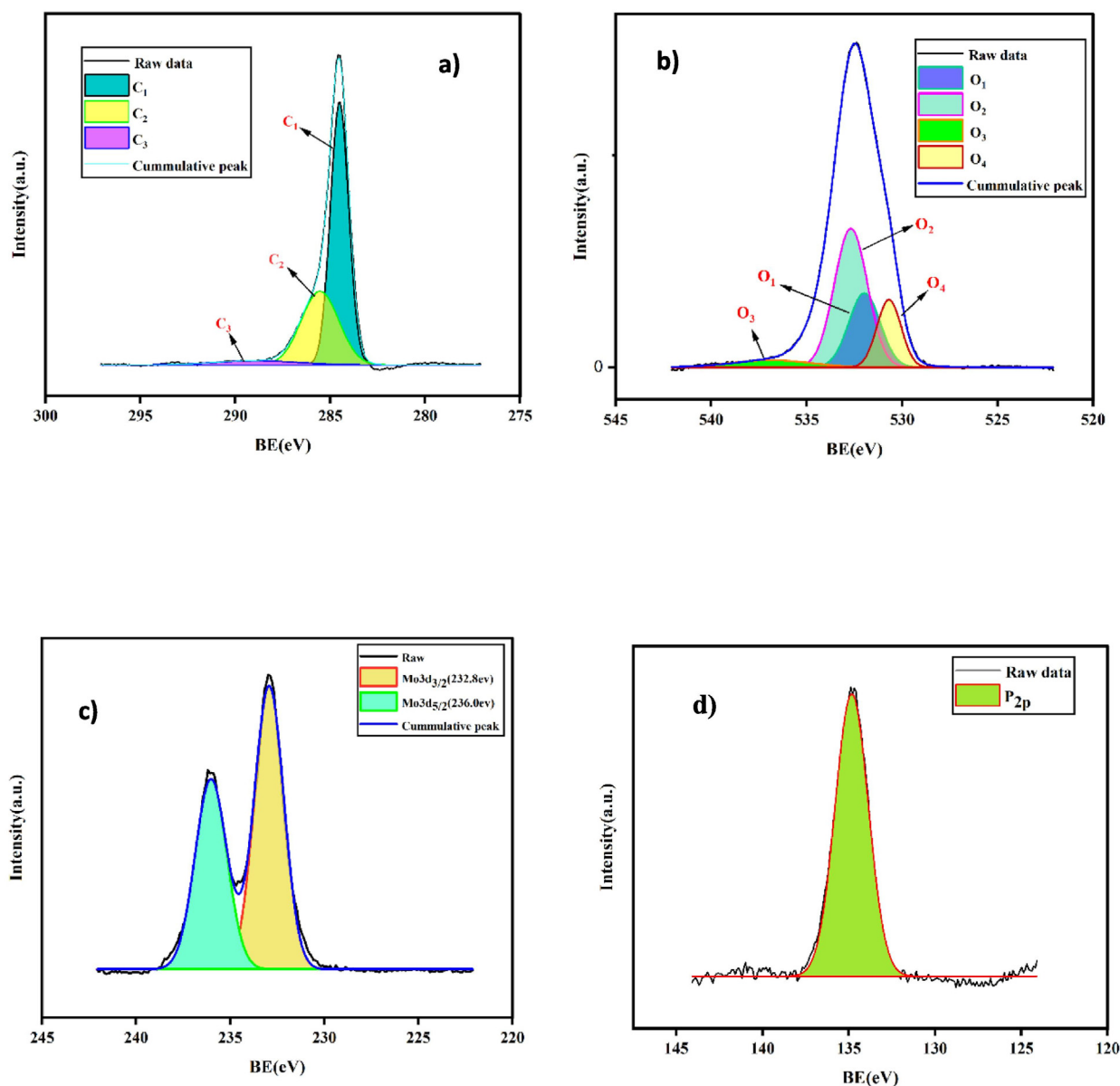


Fig. 6. XPS Analysis a) C1s b) O1s c) Mo 3d d) P2p.

have been previously reported in the literature [45]. The elemental composition of the OPAC and OPAC-PMA composite was also performed using energy-dispersive spectroscopy (EDS), as shown in Fig. 7(c & d). The composite's EDS and elemental mapping (Fig. 7 e, f, g and h) confirm the occurrence of P, Mo, O, and C.

3.6. BET surface area

The BET surface area was estimated using a Micromeritics physisorption analyzer (Model ASAP 2020, USA). The N₂ adsorption-desorption study with the OPAC-PMA composite material exhibited type I isotherm with pore-filling phenomena at a lower relative pressure ($P/P_0 < 0.1$), indicating the presence of micropores (Fig. 8a). The adsorption-desorption isotherm did not reveal well-defined hysteresis loop and capillary condensation characteristics of mesoporous pores. The micropore and BET surface area are estimated at 292 m² g⁻¹ and 596 m² g⁻¹, respectively. The average pore diameter estimated by the BJH method is ~ 3.0 nm.

3.7. Electrochemical characterisation

3.7.1. Cyclic voltammetry

Cyclic voltammetry tests (IVIUM Technologies BV Co., The Netherlands, Model: Vertex) were conducted on both the OPAC and OPAC-PMA materials in a 0.5 M H₂SO₄ electrolyte solution. As shown in Fig. 9(a), the CV curves collected at different scan rates (mV/s), such as 100, 70, 50, and 20, illustrate the rectangular shape of the OPAC material, indicating its EDLC behaviour [54]. For the OPAC-PMA composite, the same scanning rates were applied, and the results are presented in Fig. 9(b). The CV graph of OPAC-PMA observed irregular shape explains the redox behaviour originates due to the presence of pseudocapacitive material on OPAC (Fig. 9(b)). Increasing the scan rate makes it even more difficult for the electrolyte ions to diffuse into the electrode's internal structure and pores as the movements of ions increase. A weak interaction between the electrolyte and electrode materials decreases specific capacitance [55]. Fig. 9(d) illustrates the combined CV curves of OPAC, PMA, and OPAC-PMA at 100 scan rates (mV/s). Here we observed that bare OPAC exhibits the rectangular

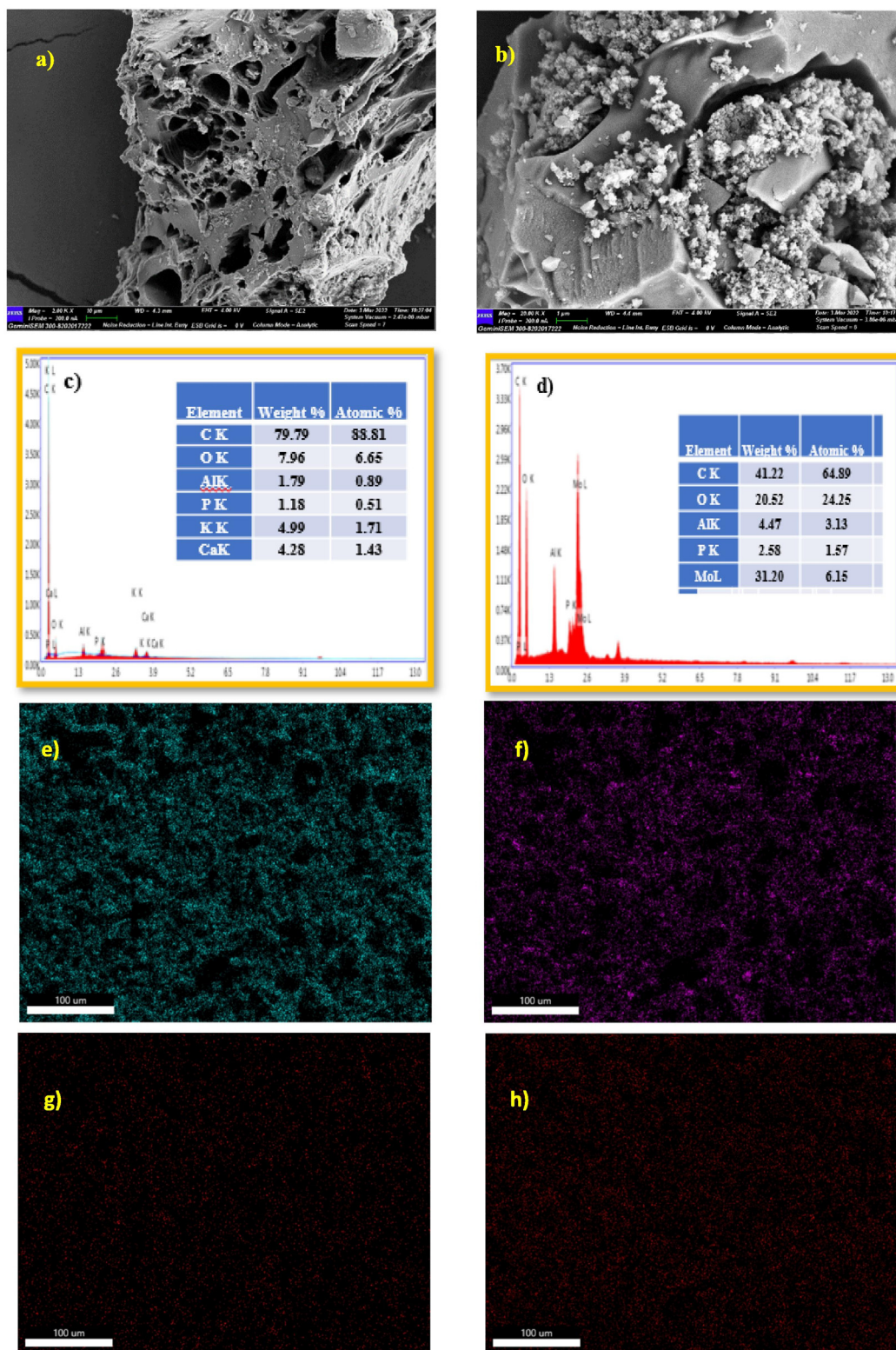


Fig. 7. a) FESEM image of OPAC, b) OPAC-PMA & c) EDS of OPAC, d) OPAC-PMA, & Elemental Mapping of e) Carbon, f) Oxygen, g) Phosphorus, h) Molybdenum.

curve, suggesting EDLC behaviour. PMA is a pseudo-type material, showing oxidation/reduction peaks in the CV curves (Fig. 9(c)). However, the OPAC-PMA display of a non-rectangular shape proves that the material undergoes the redox process. The redox peak current value is higher than the double-layer current. The OPAC-PMA composite

shows a more significant increase in current density than the pure OPAC. The bare PMA CV was performed at the same scan rates, and redox peaks are distinctively visible, illustrated in Fig. 9(c). The specific capacitance of bare OPAC, OPAC-PMA, and PMA in symmetric electrodes was calculated from the CV plots using the following equation (1):

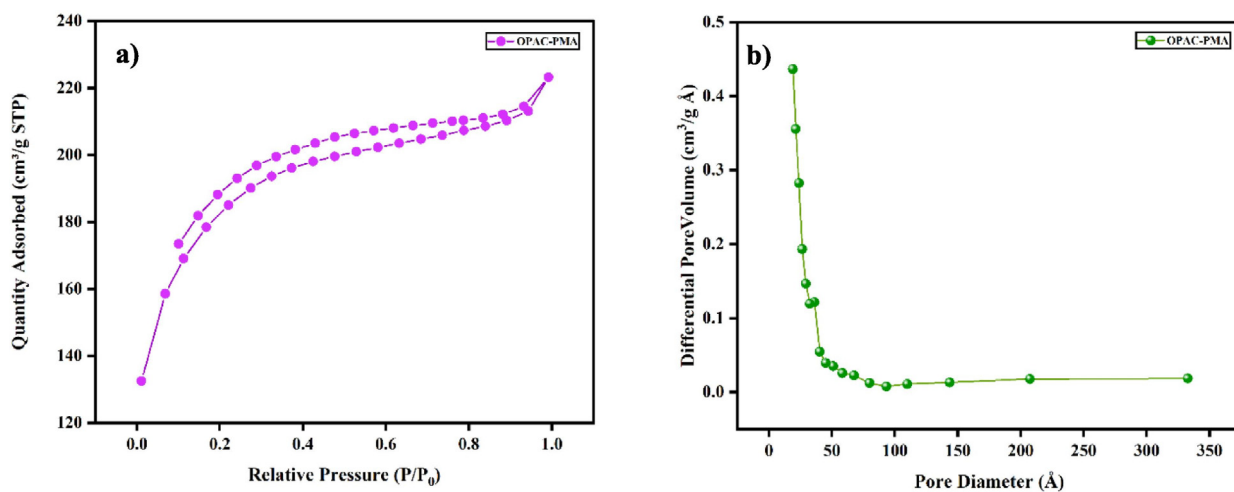


Fig. 8. a) N₂ Adsorption and desorption Isotherm & b) Pore diameter of OPAC-PMA.

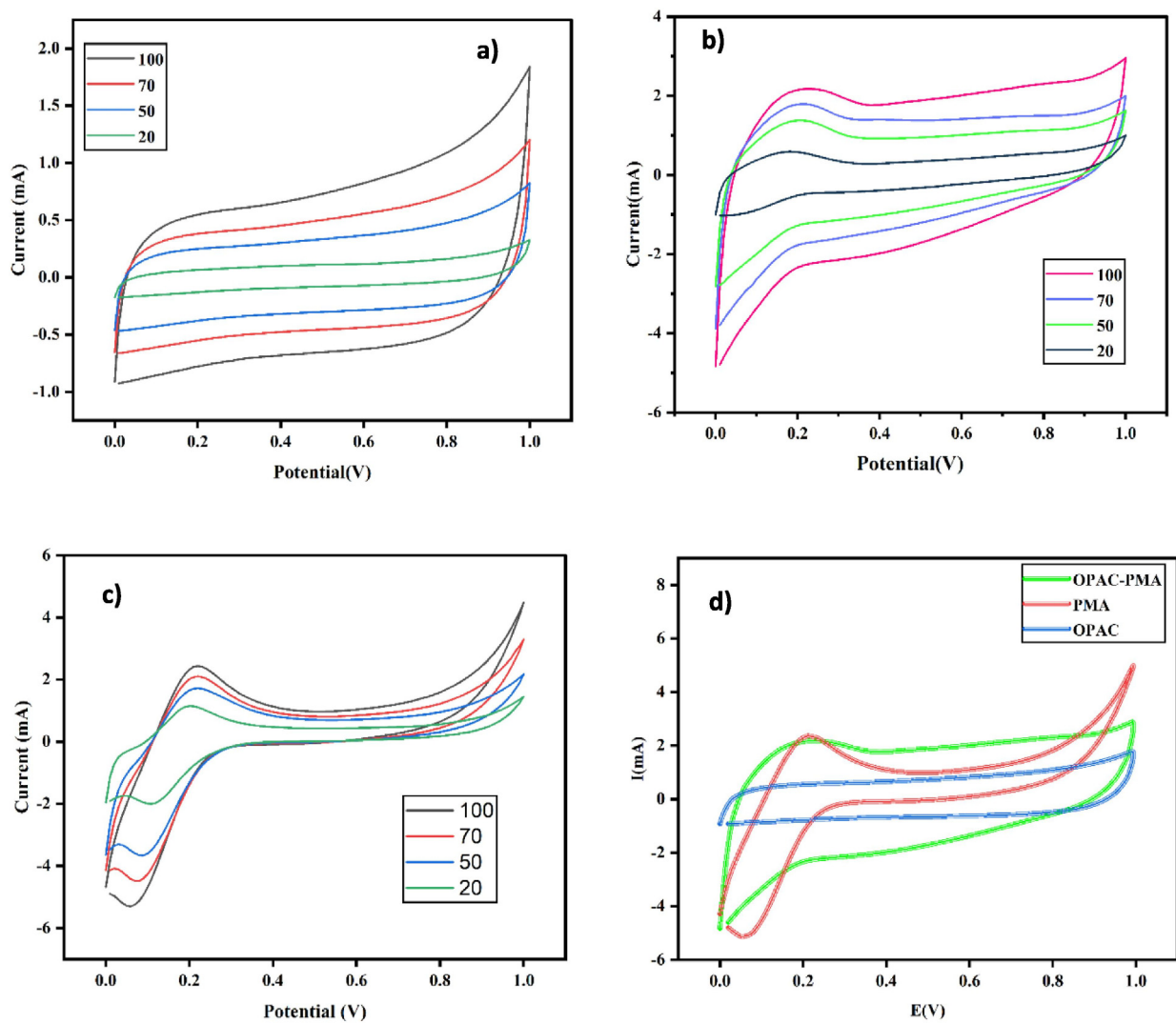


Fig. 9. Cyclic voltammety graphs a) OPAC b) OPAC-PMA c) PMA d) Combination graph of OPAC, OPAC-PMA, and PMA.

$$\text{Specific capacitance (Cs)} : C_s = \frac{1}{2m \times \nu \times \Delta V} \int I(V)dV \quad (1)$$

where m , ν , and ΔV are the active material's mass, scan rate, and potential window, respectively. The Specific capacitance and energy density of both OPAC and OPAC-PMA are presented in Fig. S2.

3.7.2. Galvanostatic charge–discharge studies

The galvanostatic charge–discharge characteristics under various current densities were studied to determine the electrode material's electrochemical behaviour under a particular potential window. A galvanostatic charge–discharge (GCD) study was conducted using a 0.5 M H_2SO_4 electrolyte solution in a two-electrode supercapacitor cell configuration. The composite showed a specific capacitance of

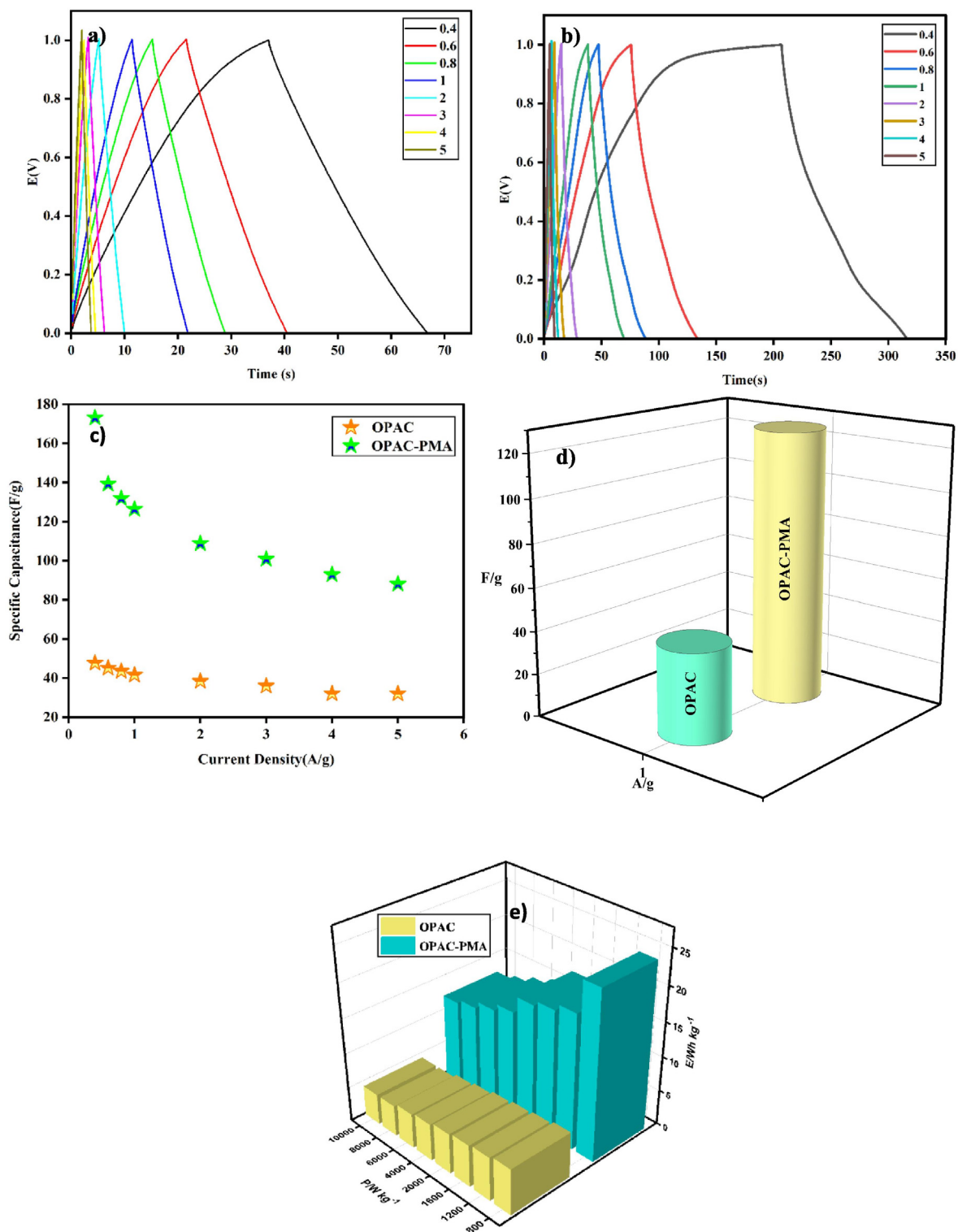


Fig. 10. GCD graph of a) OPAC b) OPAC-PMA c) Current densities vs Specific capacitance for all systems d) current density vs specific capacitance for OPAC & OPAC-PMA at 1 A g⁻¹ e) Ragone plot for OPAC & OPAC-PMA.

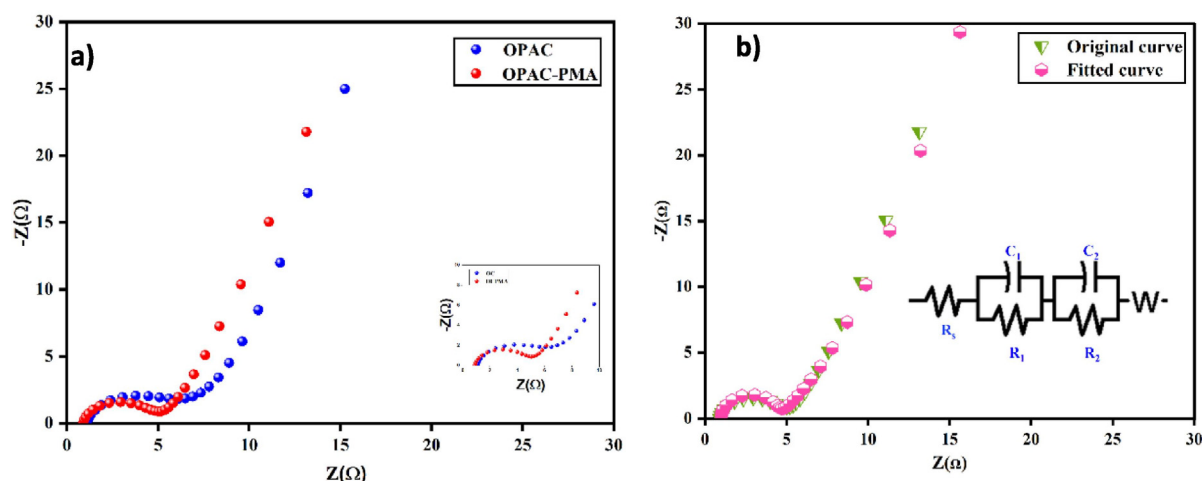


Fig. 11. a) Nyquist plot b) Fitting the Nyquist plots require using an equivalent circuit.

173.12 F g⁻¹ at a current density of 0.4 A g⁻¹ calculated using Eq. (2) with an energy and power density of 24.04 Wh kg⁻¹ & 800 W kg⁻¹. The OPAC-PMA exhibited a specific capacitance of 173.12 F g⁻¹, which is 66% higher than the bare OPAC's specific capacitance of 47.68 F g⁻¹ at the same current density. The energy and power densities of the materials were calculated using Eqs. (3) and (4), respectively. Ragone plots of OPAC and OPAC-PMA are represented in Fig. 10e. The Ragone plots demonstrate that composite OPAC-PMA has a higher energy density than OPAC. The GCD curve of OPAC exhibits the exact triangle shape, indicating high reversibility of the electrode material during the charge and discharge process, as described in Fig. 10a [56]. Whereas the shape of the GCD curve of OPAC-PMA is not a perfect triangle, indicating the oxidation/reduction process occurring in the presence of PMA, as shown in Fig. 10b. A perfectly nonlinear GCD graph of pseudocapacitive PMA because of the faradic process is shown in Fig. S4, which has been performed in the same current density and electrolyte solution. The specific capacitance of OPAC and OPAC-PMA was compared at 1 A g⁻¹, as shown in Fig. 10d, indicating a drastic increase in specific capacitance resulting from the insertion of pseudocapacitive materials (PMA) into non-faradic materials, which undergoes both redox reactions as well as charge accumulation mechanisms. It is evident that the OPAC-PMA composite exhibits higher specific capacitance than the pure OPAC. The specific capacitances, energy, and power densities for different current densities ranging from 0.4 to 4 A g⁻¹ for both OPAC and OPAC-PMA materials are tabulated in Tables S1 and S3. Notably, the OPAC-PMA sample is highly reproducible after measurements of the sample prepared under the same reaction conditions (Fig. S7 and Tables S5 & S6). The various percentage loading of PMA (10 wt% to 50 wt%) on OPAC were tested and it has been observed that the capacitance increases upto 40 wt% loading of PMA and starts decreasing with higher loading of PMA i.e., 50 wt% (Fig. S8d). Specific Capacitance (Cs /g) $C_s = i \cdot \Delta_m^{\frac{1}{2}} \cdot (\Delta V) V$

$$\text{Specific Capacitance } C_s = I \cdot \Delta t / \Delta V \text{ F/g} \quad (2)$$

$$\text{Energy density (E.D) } E = \int i V dt \text{ Wh/Kg} \quad (3)$$

$$\text{Power Density (PD) } P = \frac{E}{\Delta t(s)} \times 3600 \text{ W/Kg} \quad (4)$$

3.7.3. Electrochemical impedance study of OPAC-PMA composites

The pure OPAC and composite (OPAC-PMA) electrodes performed an electrochemical impedance spectroscopy study. A Nyquist plot can be used to determine a composite's internal resistance and its charge transfer kinetics and ion diffusion processes (Fig. 11a) [57]. Over the high-frequency region, the impedance spectroscopy results demonstrate the semicircle arc for the electrodes. Because of limited mass transport, redox reactions mediated electron transfer kinetics are visualized by measuring the impedance of the electrode-electrolyte interface at lower frequencies. [58,59]. The appearance of the partial semicircle at higher frequencies indicates the resistance to charge transfer. Here R_s represent the solution resistance, and the calculated R_s values for OPAC, OPAC-PMA, and PMA are 1.13(Ω), 0.89(Ω) (Table 1), and 0.82(Ω) (Table S4). In contrast, the calculated polarized resistance (R_p) of OPAC, OPAC-PMA, and PMA are 6.07(Ω), 5.03(Ω) (Table 1), and 6.79(Ω) (Table S4) respectively. The charge transfer resistance (R_{CT}) values of OPAC, OPAC-PMA, and PMA are 4.94(Ω), 4.13(Ω), and 5.98(Ω) (Table S4), respectively. Despite being symmetric, the OPAC-PMA electrode has a lower resistance than OPAC and PMA due to the presence of PMA, which increases the conductivity of OPAC. A schematic of the equivalent circuit for OPAC-PMA (symmetric) electrode material is presented in Fig. 11(b). The equivalent series circuit was fitted using the software Zswipwim (3.21), where R_s represents the solution resistance, C_1 & C_2 correspond to the capacitance, R_1 & R_2 are the resistances, and W represents the Warburg coefficient, which is determined by the mass transportation that occurs.

3.7.4. Cycle stability

The supercapacitor cell's stability is the most imperative characteristic of a device's application. Symmetrical electrodes, which are OPAC and OPAC-PMA, have been tested for cycle stability using GCD (Fig. 12). In an electrochemical system, OPAC-PMA electrode material

Table 1

Fitting data from Nyquist plots of equivalent circuit elements of OPAC and OPAC-PMA.

Materials	R_s (Ω)	R_p (Ω)	R_{CT} (Ω)
OPAC	1.13	6.07	4.94
OPAC-PMA	0.89	5.03	4.13

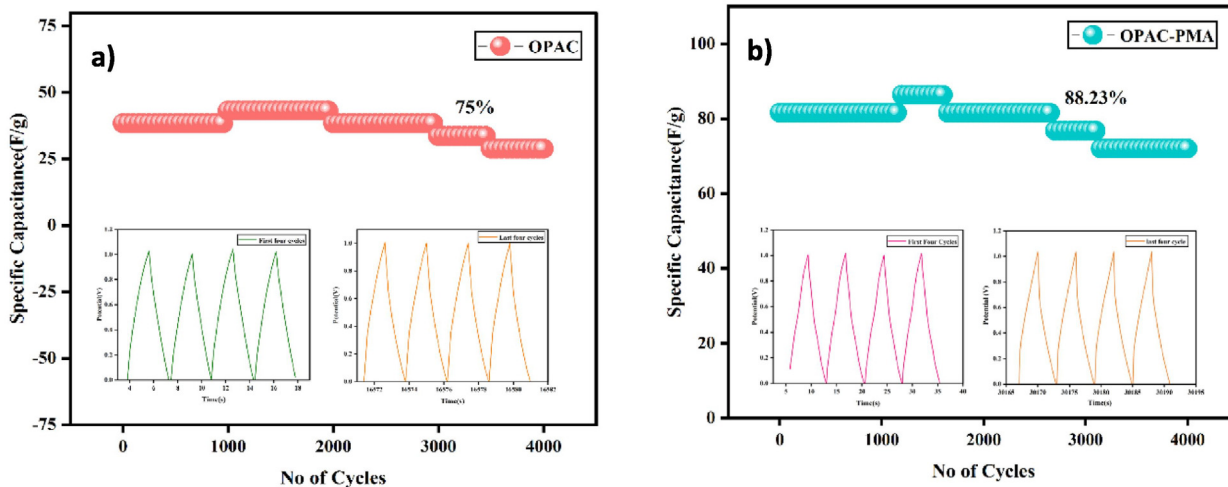


Fig. 12. The cyclic stability response of (a) OPAC and (b) OPAC-PMA for 4000 cycles at a fixed current density of 6 A g^{-1} .

exhibited outstanding cycle stability of 88.23% after 4000 cycles at 6 A g^{-1} (Fig. 12b) for a symmetrical system, demonstrating that the long-term electrochemical capacitors are unaffected by subsequent cycles and similar to the first cycle. The insert pictured in Fig. 12 (a&b) shows the nanocomposite's first and last four cycles. It has been observed that after 4000 cycles, the electrode materials are stable. Cycle stability of bare OPAC (Fig. 12a) and PMA (Fig. S6) was also performed for 4000 cycles at 6 current densities in $0.5 \text{ M H}_2\text{SO}_4$ and retained 75% and 49% respectively. To investigate the composite material's practical application, four pairs of carbon clothes ($4 \text{ cm} \times 4 \text{ cm}$) were coated with OPAC-PMA following the fabrication method described above (160 mg of active electrode material coated) and were connected in series. Using an electrochemical workstation, we charged a red LED (2 V) in a high current density of around 20 A g^{-1} at a potential window 0–3 V (Fig. 13) and lit them up. The LED continued to glow for 90 s after removing the electrochemical workstation, taking energy from the device, which proves the device's incredible power density.



Fig. 13. The fabricated supercapacitors are energizing red light-emitting diodes. (For interpretation of the references to colour in this figure legend, the reader is referred to the web version of this article.)

4. Conclusion

We successfully suffuse PMA into orange peel-derived activated carbon (OPAC) through an in-situ deposition. At a current density of 1 A g^{-1} , the electrode OPAC-PMA demonstrates a high specific capacitance of 126 F g^{-1} and the highest specific power and energy values, respectively, of 17.55 W kg^{-1} and 2000 Wh kg^{-1} . The OPAC-PMA electrode material has a capacitance value of 66% higher than the OPAC electrode. The OPAC-PMA material shows 88.23% cycle stability at 6 A g^{-1} in $0.5 \text{ M H}_2\text{SO}_4$ electrolyte for 4000 cycles. Furthermore, the OPAC-PMA electrode can illuminate a red LED bulb for more than a minute.

CRediT authorship contribution statement

Madhusree J.E.: Visualization, Investigation, Writing – original draft, Software. **Pranay R. Chandewar:** Investigation, Data curation. **Debaprasad Shee:** Writing – review & editing. **Sib Sankar Mal:** Conceptualization, Methodology, Writing – review & editing, Supervision.

Declaration of Competing Interest

The authors declare that they have no known competing financial interests or personal relationships that could have appeared to influence the work reported in this paper.

Acknowledgments

This work is supported by the Council of Scientific and Industrial Research (CSIR) under scheme 01/(2906)/17/EMR-II.

Appendix A. Supplementary data

Supplementary data to this article can be found online at <https://doi.org/10.1016/j.jelechem.2023.117354>.

References

- [1] C. Liu, F. Li, L.-P. Ma, H.-M. Cheng, *Advanced Materials for Energy Storage*, *Adv. Mater.* 22 (8) (2010) E28–E62, <https://doi.org/10.1002/adma.200903328>.
- [2] S. Koochi-Fayegh, M.A. Rosen, *A Review of Energy Storage Types, Applications and Recent Developments*, *J. Storage Mater.* 27 (2020), <https://doi.org/10.1016/j.est.2019.101047> 101047.
- [3] S. Liu, R. Zhang, J. Mao, Y. Zhao, Q. Cai, Z. Guo, *From Room Temperature to Harsh Temperature Applications: Fundamentals and Perspectives on Electrolytes in Zinc*

- Metal Batteries, *Sci. Adv.* 8 (12) (2022) eabn5097, <https://doi.org/10.1126/sciadv.abn5097>.
- [4] Li, J.; Hu, T.; Wang, Y.; Chen, S.; Wang, C.; Zhang, D.; Sun, Z.; Li, F. A Chlorine-Based Redox Electrochemical Capacitor. *ACS Appl. Mater. Interfaces* 2022, *acsami.2c03951*. 10.1021/acsami.2c03951.
- [5] Y. Shen, X. Yan, L. An, S. Shen, L. An, J. Zhang, Portable Proton Exchange Membrane Fuel Cell Using Polyoxometalates as Multi-Functional Hydrogen Carrier, *Appl. Energy* 313 (2022), <https://doi.org/10.1016/j.apenergy.2022.118781> 118781.
- [6] M. Winter, R.J. Brodd, What Are Batteries, Fuel Cells, and Supercapacitors?, *Chem Rev.* 104 (10) (2004) 4245–4270, <https://doi.org/10.1021/cr020730k>.
- [7] K. Naoi, W. Naoi, S. Aoyagi, J. Miyamoto, T. Kamino, New Generation “Nanohybrid Supercapacitor.”, *Acc. Chem. Res.* 46 (5) (2013) 1075–1083, <https://doi.org/10.1021/ar200308h>.
- [8] W. Raza, F. Ali, N. Raza, Y. Luo, K.-H. Kim, J. Yang, S. Kumar, A. Mehmood, E.E. Kwon, Recent Advancements in Supercapacitor Technology, *Nano Energy* 52 (2018) 441–473, <https://doi.org/10.1016/j.nanoen.2018.08.013>.
- [9] L.L. Zhang, X.S. Zhao, Carbon-Based Materials as Supercapacitor Electrodes, *Chem. Soc. Rev.* 38 (9) (2009) 2520, <https://doi.org/10.1039/b813846j>.
- [10] T. Purkait, G. Singh, D. Kumar, M. Singh, R.S. Dey, High-Performance Flexible Supercapacitors Based on Electrochemically Tailored Three-Dimensional Reduced Graphene Oxide Networks, *Sci. Rep.* 8 (1) (2018) 640, <https://doi.org/10.1038/s41598-017-18593-3>.
- [11] W. Tuichai, A. Karaphun, C. Ruttanapun, Ag Nanomaterials Deposited Reduced Graphene Oxide Nanocomposite as an Advanced Hybrid Electrode Material for Asymmetric Supercapacitor Device, *J. Alloy. Compd.* 849 (2020), <https://doi.org/10.1016/j.jallcom.2020.156516>.
- [12] J. Tabuchi, T. Saito, Y. Kibi, A. Ochi, Large Capacitance Electric Double Layer Capacitor Using Activated Carbon/Carbon Composite, *IEEE Trans. Comp., Hybrids, Manufact. Technol.* 16 (4) (1993) 431–436, <https://doi.org/10.1109/33.237939>.
- [13] C. Niu, E.K. Sichel, R. Hoch, D. Moy, H. Tennent, High Power Electrochemical Capacitors Based on Carbon Nanotube Electrodes, *Appl. Phys. Lett.* 70 (11) (1997) 1480–1482, <https://doi.org/10.1063/1.118568>.
- [14] F. Yu, S. Li, W. Chen, T. Wu, C. Peng, Biomass-Derived Materials for Electrochemical Energy Storage and Conversion: Overview and Perspectives, *Energy Environ. Mater.* 2 (1) (2019) 55–67, <https://doi.org/10.1002/eam2.12030>.
- [15] L. Zhang, Z. Liu, G. Cui, L. Chen, Biomass-Derived Materials for Electrochemical Energy Storages, *Prog. Polym. Sci.* 43 (2015) 136–164, <https://doi.org/10.1016/j.progpolymsci.2014.09.003>.
- [16] J. Deng, M. Li, Y. Wang, Biomass-Derived Carbon: Synthesis and Applications in Energy Storage and Conversion, *Green Chem.* 18 (18) (2016) 4824–4854, <https://doi.org/10.1039/C6GC01172A>.
- [17] N. Yadav, M.K. Singh, N. Yadav, S.A. Hashmi, High Performance Quasi-Solid-State Supercapacitors with Peanut-Shell-Derived Porous Carbon, *J. Power Sources* 402 (2018) 133–146, <https://doi.org/10.1016/j.jpowsour.2018.09.032>.
- [18] F. Guo, X. Jiang, X. Li, K. Peng, C. Guo, Z. Rao, Carbon Electrode Material from Peanut Shell by One-Step Synthesis for High Performance Supercapacitor, *J. Mater. Sci. Mater. Electron.* 30 (1) (2019) 914–925, <https://doi.org/10.1007/s10854-018-0362-9>.
- [19] A. Tripathy, S. Mohanty, S.K. Nayak, A. Ramadoss, Renewable Banana-Peel-Derived Activated Carbon as an Inexpensive and Efficient Electrode Material Showing Fascinating Supercapacitive Performance, *J. Environ. Chem. Eng.* 9 (6) (2021), <https://doi.org/10.1016/j.jece.2021.106398> 106398.
- [20] Y. Zhang, Z. Gao, N. Song, X. Li, High-Performance Supercapacitors and Batteries Derived from Activated Banana-Peel with Porous Structures, *Electrochim. Acta* 222 (2016) 1257–1266, <https://doi.org/10.1016/j.electacta.2016.11.099>.
- [21] G. Bharath, A. Hai, K. Rambabu, F. Ahmed, A.S. Haidyrah, N. Ahmad, S.W. Hasan, F. Banat, Hybrid Capacitive Deionization of NaCl and Toxic Heavy Metal Ions Using Faradic Electrodes of Silver Nanospheres Decorated Pomegranate Peel-Derived Activated Carbon, *Environ. Res.* 197 (2021), <https://doi.org/10.1016/j.envres.2021.111110> 111110.
- [22] K. Sun, J. Li, H. Peng, E. Feng, G. Ma, Z. Lei, Promising Nitrogen-Doped Porous Nanosheets Carbon Derived from Pomegranate Husk as Advanced Electrode Materials for Supercapacitors, *Ionics* 23 (4) (2017) 985–996, <https://doi.org/10.1007/s11581-016-1897-5>.
- [23] J. Choi, T. Wixson, A. Worsley, S. Dhungana, S.R. Mishra, F. Perez, R.K. Gupta, Pomegranate: An Eco-Friendly Source for Energy Storage Devices, *Surf. Coat. Technol.* 421 (2021), <https://doi.org/10.1016/j.surfcoat.2021.127405> 127405.
- [24] K.-C. Lee, M.S.W. Lim, Z.-Y. Hong, S. Chong, T.J. Tiong, G.-T. Pan, C.-M. Huang, Coconut Shell-Derived Activated Carbon for High-Performance Solid-State Supercapacitors, *Energies* 14 (15) (2021) 4546, <https://doi.org/10.3390/en14154546>.
- [25] H. Chen, Y. Zheng, X. Zhu, W. Hong, Y. Tong, Y. Lu, G. Pei, Y. Pang, Z. Shen, C. Guan, Bamboo-Derived Porous Carbons for Zn-Ion Hybrid Supercapacitors, *Mater. Res. Bull.* 139 (2021), <https://doi.org/10.1016/j.materresbull.2021.111281>.
- [26] H. Chen, D. Liu, Z. Shen, B. Bao, S. Zhao, L. Wu, Functional Biomass Carbons with Hierarchical Porous Structure for Supercapacitor Electrode Materials, *Electrochim. Acta* 180 (2015) 241–251, <https://doi.org/10.1016/j.electacta.2015.08.133>.
- [27] S. Yu, D. Liu, S. Zhao, B. Bao, C. Jin, W. Huang, H. Chen, Z. Shen, Synthesis of Wood Derived Nitrogen-Doped Porous Carbon-Polyaniline Composites for Supercapacitor Electrode Materials, *RSC Adv.* 5 (39) (2015) 30943–30949, <https://doi.org/10.1039/C5RA01949D>.
- [28] G. Lou, G. Pei, Y. Wu, Y. Lu, Y. Wu, X. Zhu, Y. Pang, Z. Shen, Q. Wu, S. Fu, H. Chen, Combustion Conversion of Wood to N, O Co-Doped 2D Carbon Nanosheets for Zinc-Ion Hybrid Supercapacitors, *Chem. Eng. J.* 413 (2021), <https://doi.org/10.1016/j.cej.2020.127502> 127502.
- [29] X. Zhu, S. Yu, K. Xu, Y. Zhang, L. Zhang, G. Lou, Y. Wu, E. Zhu, H. Chen, Z. Shen, B. Bao, S. Fu, Sustainable Activated Carbons from Dead Ginkgo Leaves for Supercapacitor Electrode Active Materials, *Chem. Eng. Sci.* 181 (2018) 36–45, <https://doi.org/10.1016/j.ces.2018.02.004>.
- [30] C. Largeot, C. Portet, J. Chmiola, P.-L. Taberna, Y. Gogotsi, P. Simon, Relation between the Ion Size and Pore Size for an Electric Double-Layer Capacitor, *J. Am. Chem. Soc.* 130 (9) (2008) 2730–2731, <https://doi.org/10.1021/ja7106178>.
- [31] F. Boorboor Ajdari, E. Kowsari, A. Ehsani, P-Type Conductive Polymer/Zeolitic Imidazolate Framework-67 (ZIF-67) Nanocomposite Film: Synthesis, Characterization, and Electrochemical Performance as Efficient Electrode Materials in Pseudocapacitors, *J. Colloid Interface Sci.* 509 (2018) 189–194, <https://doi.org/10.1016/j.jcis.2017.08.098>.
- [32] D. Cheng, Y. Yang, J. Xie, C. Fang, G. Zhang, J. Xiong, Hierarchical NiCo₂O₄@NiMoO₄ Core-Shell Hybrid Nanowire/Nanosheet Arrays for High-Performance Pseudocapacitors, *J. Mater. Chem. A* 3 (27) (2015) 14348–14357, <https://doi.org/10.1039/C5TA03455H>.
- [33] Y. Zhao, J. Liu, Y. Hu, H. Cheng, C. Hu, C. Jiang, L. Jiang, A. Cao, L. Qu, Highly Compression-Tolerant Supercapacitor Based on Polypyrrole-Mediated Graphene Foam Electrodes, *Adv. Mater.* 25 (4) (2013) 591–595, <https://doi.org/10.1002/adma.201203578>.
- [34] Y. Lee, S. Kim, J.H. Lee, K.C. Roh, E. Lim, J. Lee, Improved Pseudocapacitive Charge Storage in Highly Ordered Mesoporous TiO₂/Carbon Nanocomposites as High-Performance Li-Ion Hybrid Supercapacitor Anodes, *RSC Adv.* 9 (65) (2019) 37882–37888, <https://doi.org/10.1039/C9RA07157A>.
- [35] J. Jacob, P. Preetha, S. Thiruthi Krishnan, Review on Natural Ester and Nanofluids as an Environmental Friendly Alternative to Transformer Mineral Oil, *IET Nanodielectrics* 3 (2) (2020) 33–43, <https://doi.org/10.1049/iet-nde.2019.0038>.
- [36] N.I. Gumerova, A. Rompel, Synthesis, Structures and Applications of Electron-Rich Polyoxometalates, *Nat. Rev. Chem.* 2 (2) (2018) 0112, <https://doi.org/10.1038/s41570-018-0112>.
- [37] M.I.S. Verissimo, D.V. Evtuguin, M.T.S.R. Gomes, Polyoxometalate Functionalized Sensors: A Review, *Front. Chem.* 10 (2022), <https://doi.org/10.3389/fchem.2022.840657> 840657.
- [38] Wang, S.-S.; Yang, G.-Y. Recent Advances in Polyoxometalate-Catalyzed Reactions. *Chem. Rev.* 2015, 115 (11), 4893–4962. 10.1021/cr500390v. (41) Long, D.-L.; Tsunashima, R.; Cronin, L. Polyoxometalates: Building Blocks for Functional Nanoscale Systems. *Angew. Chem. Int. Ed.* 2010, 49 (10), 1736–1758. 10.1002/anie.200902483
- [39] D.-L. Long, R. Tsunashima, L. Cronin, Polyoxometalates: Building Blocks for Functional Nanoscale Systems, *Angew. Chem. Int. Ed.* 49 (10) (2010) 1736–1758, <https://doi.org/10.1002/anie.200902483>.
- [40] H. Wang, S. Hamanaka, Y. Nishimoto, S. Irlé, T. Yokoyama, H. Yoshikawa, K. Awaga, In Operando X-Ray Absorption Fine Structure Studies of Polyoxometalate Molecular Cluster Batteries: Polyoxometalates as Electron Sponges, *J. Am. Chem. Soc.* 134 (10) (2012) 4918–4924, <https://doi.org/10.1021/ja2117206>.
- [41] M. Genovese, Y.W. Foong, K. Lian, The Unique Properties of Aqueous Polyoxometalate (POM) Mixtures and Their Role in the Design of Molecular Coatings for Electrochemical Energy Storage, *Electrochim. Acta* 199 (2016) 261–269, <https://doi.org/10.1016/j.electacta.2016.01.145>.
- [42] M. Genovese, K. Lian, Polyoxometalate Modified Pine Cone Biochar Carbon for Supercapacitor Electrodes, *J. Mater. Chem. A* 5 (8) (2017) 3939–3947, <https://doi.org/10.1039/C6TA10382K>.
- [43] A. Pandiarajan, R. Kamaraj, S. Vasudevan, S. Vasudevan, OPAC (Orange Peel Activated Carbon) Derived from Waste Orange Peel for the Adsorption of Chlorophenoxyacetic Acid Herbicides from Water: Adsorption Isotherm, Kinetic Modelling and Thermodynamic Studies, *Bioresour. Technol.* 261 (2018) 329–341, <https://doi.org/10.1016/j.biortech.2018.04.005>.
- [44] C.K. Ranaweera, P.K. Kahol, M. Ghimire, S.R. Mishra, R.K. Gupta, Orange-Peel-Derived Carbon: Designing Sustainable and High-Performance Supercapacitor Electrodes, *C* 3 (4) (2017) 25, <https://doi.org/10.3390/c3030025>.
- [45] S. Kaipannan, S. Marappan, Fabrication of 9.6 V High-Performance Asymmetric Supercapacitors Stack Based on Nickel Hexacyanoferrate-Derived Ni (OH)₂ Nanosheets and Bio-Derived Activated Carbon, *Sci. Rep.* 9 (1) (2019) 1104, <https://doi.org/10.1038/s41598-018-37566-8>.
- [46] K. Subramani, N. Sudhan, M. Karnan, M. Sathish, Orange Peel Derived Activated Carbon for Fabrication of High-Energy and High-Rate Supercapacitors, *ChemistrySelect* 2 (35) (2017) 11384–11392, <https://doi.org/10.1002/slct.201701857>.
- [47] A.V. Murugan, C.-W. Kwon, G. Campet, B.B. Kale, Synthesis and Characterization of Novel Organo-Inorganic Hybrid Material of Poly(3,4-Ethylene Dioxathiophene) and Phosphomolybdate Anion, *Act. Passiv. Electron. Compon.* 26 (2) (2003) 81–86, <https://doi.org/10.1080/0882751031000073896>.
- [48] Tírhá L P Dantas; Alírio E Rodrigues; Moreira, R. F. P. M. Separation of Carbon Dioxide from Flue Gas Using Adsorption on Porous Solids. 2012. 10.13140/2.1.2092.6404.
- [49] J.-M. Taibouët, C. Montalescot, K. Brückman, J. Haber, M. Che, A Two-Step Transformation of the Magnesium Salt of Phosphomolybdic Acid HMgPMo₁₂O₄₀ Supported on Silica, *J. Catal.* 169 (1) (1997) 22–32, <https://doi.org/10.1006/jcat.1997.1693>.
- [50] Salgado, M. de F.; Abioye, A. M.; Junoh, M. M.; Santos, J. A. P.; Ani, F. N. Preparation of Activated Carbon from Babassu Endocarp under Microwave

- Radiation by Physical Activation. IOP Conf. Ser.: Earth Environ. Sci. **2018**, *105*, 012116. 10.1088/1755-1315/105/1/012116.
- [51] A. Bazan, P. Nowicki, P. Pótrolniczak, R. Pietrzak, Thermal Analysis of Activated Carbon Obtained from Residue after Supercritical Extraction of Hops, *J. Therm. Anal. Calorim.* **125** (3) (2016) 1199–1204, <https://doi.org/10.1007/s10973-016-5419-5>.
- [52] Awitdrus; Siregar, G. M. G.; Agustino; Saktioto; Iwantonio; Syahputra, R. F.; Farma, R. KOH Activation with Microwave Irradiation and Its Effect on the Physical Properties of Orange Peel Activated Carbon. *J. Phys.: Conf. Ser.* **2021**, *2049* (1), 012025. 10.1088/1742-6596/2049/1/012025.
- [53] X. Wang, X. Zhang, X. He, A. Ma, L. Le, S. Lin, Facile Electrodeposition of Flower-Like PMo12-Pt/RGO Composite with Enhanced Electrocatalytic Activity towards Methanol Oxidation, *Catalysts* **5** (3) (2015) 1275–1288, <https://doi.org/10.3390/catal5031275>.
- [54] N. Elgrishi, K.J. Rountree, B.D. McCarthy, E.S. Rountree, T.T. Eisenhart, J.L. Dempsey, A Practical Beginner's Guide to Cyclic Voltammetry, *J. Chem. Educ.* **95** (2) (2018) 197–206, <https://doi.org/10.1021/acs.jchemed.7b00361>.
- [55] Markoulidis; Todorova; Grilli; Lekakou; Trapalis. Composite Electrodes of Activated Carbon and Multiwall Carbon Nanotubes Decorated with Silver Nanoparticles for High Power Energy Storage. *J. Compos. Sci.* **2019**, *3* (4), 97. 10.3390/jcs3040097
- [56] K. Bohinc, V. Kralj-Iglič, A. Iglič, Thickness of Electrical Double Layer. Effect of Ion Size, *Electrochimica Acta* **46** (19) (2001) 3033–3040, [https://doi.org/10.1016/S0013-4686\(01\)00525-4](https://doi.org/10.1016/S0013-4686(01)00525-4).
- [57] S. Muduli, V. Naresh, S.K. Martha, Boron, Nitrogen-Doped Porous Carbon Derived from Biowaste Orange Peel as Negative Electrode Material for Lead-Carbon Hybrid Ultracapacitors, *J. Electrochem. Soc.* **167** (9) (2020), <https://doi.org/10.1149/1945-7111/ab829f> 090512.
- [58] M.F. Mousavi, M. Hashemi, M.S. Rahmanifar, A. Noori, Synergistic Effect between Redox Additive Electrolyte and PANI-RGO Nanocomposite Electrode for High Energy and High Power Supercapacitor, *Electrochim. Acta* **228** (2017) 290–298, <https://doi.org/10.1016/j.electacta.2017.01.027>.
- [59] S. Zhu, M. Wu, M.-H. Ge, H. Zhang, S.-K. Li, C.-H. Li, Design and Construction of Three-Dimensional CuO/Polyaniline/RGO Ternary Hierarchical Architectures for High Performance Supercapacitors, *J. Power Sources* **306** (2016) 593–601, <https://doi.org/10.1016/j.jpowsour.2015.12.059>.